PERGAMON

International Journal of Heat and Mass Transfer 44 (2001) 1687–1697

International Journal of HEAT and MASS TRANSFER

www.elsevier.com/locate/ijhmt

A new model for heat transfer of fins swinging back and forth in a flow

Wu-Shung Fu *, Suh-Jenq Yang

Department of Mechanical Engineering, National Chiao Tung University, 1001 Ta Hsueh Road, Hsinchu 30056, Taiwan, ROC

Received 11 April 2000; received in revised form 22 June 2000

Abstract

In this paper, a new concept of an electronic device cooling method is proposed. In this method, extremely thin fins are used for swinging back and forth in a flowing fluid. The boundary layers attaching on the fins are then contracted and disturbed, and the heat transfer rate of the fins can be enhanced remarkably. The dynamic behavior between the fins and fluid is classified into a class of the moving boundary problems. A Galerkin finite element formulation with an arbitrary Lagrangian–Eulerian kinematic description method is adopted to solve this problem. The parameters of velocities of the fluid and the swinging speed of the fins are employed to investigate the variations of the flow and thermal fields. The results show that the velocity and thermal boundary layers may be contracted and disturbed, which results in a significant heat transfer enhancement, being attained.

1. Introduction

Accompanying with the progress of the semiconductor technology, the miniaturization of components becomes a trend of development of a new electronic device that results in large heat rate being generated per unit area and the temperature of the electronic device being high. The performance and reliability of the electronic device are deeply affected by its temperature. Therefore, how to control the thermal dissipation and enhance the heat transfer rate from a small size electronic device effectively becomes a very important subject.

In general, the techniques for enhancing the heat transfer are divided into two parts: ''passive'' and ''active'' methods [1,2], and both these methods have been massively used to enhancing the heat transfer of high power electronic devices. Yeh [3] summarized and reviewed the results of recent developments and researches of the heat transfer technologies in electronic equipment, such as air cooling, liquid cooling, jet impingement, heat pipe, micro-channel cooling and phases change. Sathe and Sammakia [4] made a survey of recent developments in detail for air cooling method in electronic packages.

One of the above technologies of adding a finned heat sink on a hot component to enlarge the heat transfer area for enhancing the thermal performance is universally employed in the electronic device and heat exchangers, and several papers [5–8] had studied in this topic. Furthermore, vibrating a heated body surface also is an effective method to enhance the heat transfer rate and had been studied experimentally and theoretically [9–13], and the results indicated the heat transfer rate of the heated body to be increased remarkably.

However, at present it appears that the heat transfer efficiency of the finned heat sink may fail to catch up with the increasing rate of the heat generation of a new electronic device. As for the method of vibrating of the heated body surface, it seriously reduces the reliability and stability of the electronic device.

Thus, a new cooling concept, in which the fins of the finned heat sink swing back and forth in flowing fluid, is proposed to enhance the heat transfer of the high power electronic device reliably and stably. For realizing this concept, the fins of the finned heat sink are needed to be made of extremely thin metal, then these thin fins could be easily swinging back and forth by the flowing fluid, or

* Corresponding author. Tel.: +886-3-5712121/5510; fax: +886-3-5720634.

E-mail address: wsfu@cc.nctu.edu.tw (W.-S. Fu).

0017-9310/01/$ - see front matter
PII: S0017-9310(00)00220-9

Nomenclature

d	dimensional thickness of the fins (m)
D	dimensionless thickness of the fins ($D = d/w_2$)
h	dimensional width of the channel (m)
H	dimensionless width of the channel ($H = h/w_2$)
h_1	dimensional distance from the wall of the channel to the fins (m)
H_1	dimensionless distance from the wall of the channel to the fins ($H_1 = h_1/w_2$)
h_2	dimensional pitch of the fins (m)
H_2	dimensionless pitch of the fins ($H_2 = h_2/w_2$)
N_i	shape function
n	normal vector of coordinates
n_e	number of elements
Nu	overall average Nusselt number of the fins
Nu_X	local Nusselt number on the top or bottom surface of the fins
$\overline{Nu_X}$	average Nusselt number on the top or bottom surface of the fins
p	dimensional pressure (N m^{-2})
p_∞	referential pressure (N m^{-2})
P	dimensionless pressure ($P = (p - p_\infty)/\rho u_0^2$)
Pr	Prandtl number ($Pr = \alpha/v$)
Re	Reynolds number ($Re = u_0 w_2/v$)
Re_ι	Reynolds number for the Blasius solution ($Re_\iota = u_0 \iota/v$)
s_b	dimensional swinging speed of the fins (m s^{-1})
S_b	dimensionless swinging speed of the fins ($S_b = s_b/u_0$)
t	dimensional time (s)
T	dimensional temperature (°C)
T_f	dimensional temperature of the fins (°C)
T_0	dimensional temperature of the inlet fluid (°C)
u, v	dimensional velocities in x- and y-directions (m s^{-1})
U, V	dimensionless velocities in X- and Y-directions ($U = u/u_0, V = v/u_0$)
u_0	dimensional velocity of the inlet fluid (m s^{-1})
v_b	dimensional swinging velocity of the fins (m s^{-1})
V_b	dimensionless swinging velocity of the fins ($V_b = v_b/u_0$)
$\hat{v}$	dimensional mesh velocity in y-direction (m s^{-1})
$\hat{V}$	dimensionless mesh velocity in Y-direction ($\hat{V} = \hat{v}/u_0$)
w	dimensional length of the channel (m)
W	dimensionless length of the channel ($W = w/w_2$)
w_1	dimensional distance from the inlet to the front side of the fins (m)
W_1	dimensionless distance from the inlet to the front side of the fins ($W_1 = w_1/w_2$)
w_2	dimensional length of the fins (m)
W_2	dimensionless length of the fins ($W_2 = w_2/w_2$)
x, y	dimensional Cartesian coordinates (m)
X, Y	dimensionless Cartesian coordinates ($X = x/w_2, Y = y/w_2$)

Greek symbols

α	thermal diffusivity (m^2 s^{-1})
ϕ	computational variables
ι	the length of a flat plate for the Blasius solution (m)
λ	penalty parameter
v	kinematic viscosity (m^2 s^{-1})
θ	dimensionless temperature ($\theta = (T - T_0)/(T_f - T_0)$)
ρ	density (kg m^{-3})
τ	dimensionless time ($\tau = tu_0/w_2$)

Superscripts

(e)	element
m	iteration number
T	transpose matrix

Other

[]	matrix
{}	column vector
⟨⟩	row vector

these thin fins are forced to be oscillated by an oscillation exciter installed at a proper place. As this apparatus is executed, the velocity and thermal boundary layers attached on the fins are contracted and disturbed drastically because of the swinging of the fins, which naturally results in the heat transfer rate being enhanced remarkably.

Due to the interaction between the flowing fluid and swinging fins, the variations of the flow and thermal fields become time-dependent, and this behavior belongs to a class of the moving boundary problems, which is hardly analyzed by either the Lagrangian or Eulerian kinematic description method solely. From the physical point of view, for analyzing the above phenomena validly, the moving interfaces between the fluid and fins have to be taken into consideration. An arbitrary Lagrangian–Eulerian (ALE) kinematic description method [14–19], in which the computational meshes may move with the fluid, be held fixed, or be moved in any other prescribed way, is an appropriate kinematic description method to analyze this new cooling concept mentioned above.

Consequently, the ALE kinematic description method is adopted to describe the variations of the flow

and thermal fields induced by the interaction between the swinging fins and flowing fluid and the enhancement of heat transfer of the fins numerically. A Galerkin finite element method and a backward difference scheme, dealing with the time terms, are used to solve the governing equations. Several different flow rates and swinging speeds of the fins are considered in this study.

2. Physical model

A two-dimensional horizontal channel with width h and length w as sketched in Fig. 1 is used in this study. Three extremely thin fins with thickness d and length w_2 are arranged with a pitch of h_2 in the channel. The ratio of d to w_2 is about 0.01. The distance from the inlet to the front surface of the fin is w_1, and the distance from the wall of the channel to the fin is h_1. The inlet velocity and temperature of the fluid are uniform and equal to u_0 and T_0, respectively. These fins are made of high conductivity material and maintain at a constant temperature T_f, which is higher than T_0. Initially ($t = 0$), these thin fins are assumed to be stationary and the fluid is flowing steadily. As the time $t > 0$, these thin fins are swung back and forth induced by the flowing fluid or an oscillation exciter (the photograph of the swinging fin is showed in Appendix A). Then, the variations of the flow and thermal fields become time-dependent and catalog to a class of the moving boundary problems. As a result, the ALE method is properly utilized to analyze this subject. The detail of the ALE kinematic description method is delineated in Hughes et al. [15], Donea et al. [16], and Ramaswamy and Kawahara [17].

In order to facilitate the analysis, the following assumptions are made.

1. The fluid is air and the flow field is two-dimensional, incompressible and laminar.
2. The fluid properties are constant and the effect of the gravity is neglected.
3. The moving direction of the fins is in y-direction only, and the fins oscillate with a constant swinging speed s_b.
4. The no-slip condition is held on the interfaces between the fluid and fins.

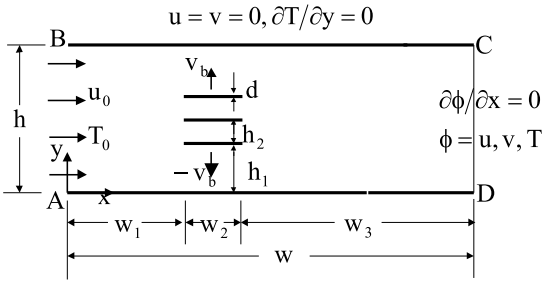

Fig. 1. Physical model.

Based upon the characteristic scales of $w_2, u_0, \rho u_0^2$ and T_0, the dimensionless variables are defined as follows:

$$X = \frac{x}{w_2}, \quad Y = \frac{y}{w_2}, \quad U = \frac{u}{u_0}, \quad V = \frac{v}{u_0}, \quad \hat{V} = \frac{\hat{v}}{u_0},$$
$$V_b = \frac{v_b}{u_0}, \quad P = \frac{p - p_\infty}{\rho u_0^2}, \quad \tau = \frac{t u_0}{w_2}, \quad \theta = \frac{T - T_0}{T_f - T_0},$$
$$Re = \frac{u_0 w_2}{\nu}, \quad Pr = \frac{\nu}{\alpha}, \tag{1}$$

where $\hat{v}$ is the mesh velocity and v_b is the swinging velocity of the fins.

According to the above assumptions and dimensionless variables, the dimensionless ALE governing equations [16–19] are expressed as the following equations:

continuity equation

$$\frac{\partial U}{\partial X} + \frac{\partial V}{\partial Y} = 0 \tag{2}$$

momentum equations

$$\frac{\partial U}{\partial \tau} + U\frac{\partial U}{\partial X} + (V - \hat{V})\frac{\partial U}{\partial Y} = -\frac{\partial P}{\partial X} + \frac{1}{Re}\left(\frac{\partial^2 U}{\partial X^2} + \frac{\partial^2 U}{\partial Y^2}\right) \tag{3}$$

$$\frac{\partial V}{\partial \tau} + U\frac{\partial V}{\partial X} + (V - \hat{V})\frac{\partial V}{\partial Y} = -\frac{\partial P}{\partial Y} + \frac{1}{Re}\left(\frac{\partial^2 V}{\partial X^2} + \frac{\partial^2 V}{\partial Y^2}\right), \tag{4}$$

energy equation

$$\frac{\partial \theta}{\partial \tau} + U\frac{\partial \theta}{\partial X} + (V - \hat{V})\frac{\partial \theta}{\partial Y} = \frac{1}{Pr\,Re}\left(\frac{\partial^2 \theta}{\partial X^2} + \frac{\partial^2 \theta}{\partial Y^2}\right). \tag{5}$$

As the time $\tau > 0$, the boundary conditions are as follows: on the fluid inlet surface AB (excluding the points A and B)

$$U = 1, \quad V = 0, \quad \theta = 0 \tag{6}$$

on the wall surfaces of the channel BC and AD

$$U = V = 0, \quad \partial\theta/\partial n = 0, \tag{7}$$

on the fluid outlet surface CD (excluding the point C and D)

$$\partial U/\partial n = \partial V/\partial n = \partial\theta/\partial n = 0, \tag{8}$$

on the interfaces between the fluid and fins

$$U = 0, \quad V = V_b, \quad \theta = 1. \tag{9}$$

3. Numerical method

A Galerkin finite element method and a backward scheme, dealing with the time terms, are adopted to solve the governing equations (2)–(5). The Newton–

Raphson iteration algorithm and a penalty function model [20] are utilized to simplify the nonlinear and pressure terms in the momentum equations, respectively. The velocity and temperature terms are approximated by quadrilateral and nine-node quadratic isoparametric elements. The discretization processes of the governing equations are similar to the one used in Fu et al. [21]. Then, the momentum equation (3) and (4) can be expressed as the following matrix form:

$$\sum_{1}^{n_e}([A]^{(e)} + [K]^{(e)} + \lambda[L]^{(e)})\{q\}^{(e)}_{\tau+\Delta\tau} = \sum_{1}^{n_e}\{f\}^{(e)}, \tag{10}$$

where

$$(\{q\}^{(e)}_{\tau+\Delta\tau})^{T} = \langle U_1, U_2, \ldots, U_9, V_1, V_2, \ldots, V_9\rangle^{m+1}_{\tau+\Delta\tau}, \tag{11}$$

$[A]^{(e)}$ consists of the (m)th iteration values of U and V at time $\tau\Delta\tau$, $[K]^{(e)}$ consists of the shape function $N_i, \hat{V}$ and time differential terms, $[L]^{(e)}$ consists of the penalty function terms, $\{f\}^{(e)}$ consists of the known values of U and V at time τ and (m)th iteration values of U and V at time $\tau + \Delta\tau$.

The energy equation (5) can be expressed as the following matrix form:

$$\sum_{1}^{n_e}([M]^{(e)} + [Z]^{(e)})\}\{c\}^{(e)}_{\tau+\Delta\tau} = \sum_{1}^{n_e}\{r\}^{(e)}, \tag{12}$$

where

$$(\{c\}^{(e)}_{\tau+\Delta\tau})^{T} = \langle\theta_1, \theta_2, \ldots x, \theta_9\rangle_{\tau+\Delta\tau}, \tag{13}$$

$[M]^{(e)}$ consists of the values of U and V at time $\tau + \Delta\tau$, $[Z]^{(e)}$ consists of the shape function $N_i, \hat{V}$ and time differential terms, $\{r\}^{(e)}$ consists of the known values of θ at time τ.

In Eqs. (10) and (12), Gaussian quadrature procedure are conveniently used to execute the numerical integration. The terms with the penalty parameter λ are integrated by 2×2 Gaussian quadrature, and the other terms are integrated by 3×3 Gaussian quadrature. The value of penalty parameter λ used in this study is 10^6. The frontal method solver [22,23] is applied to solve Eqs. (10) and (12).

The mesh velocity $\hat{V}$ is linearly distributed and inversely proportional to the distance between the nodes and fins. In addition, the boundary layer thickness on the fins surface are extremely thin and can be approximately estimated by $Re^{-1/2}$ [24]. To avoid the computational nodes in the vicinity of the fins to slip away from the boundary layer, the mesh velocity adjacent to the fins are expediently assigned equal to the velocity of the fins.

A brief outline of the solution procedure is described as follows:

1. Determine the optimal mesh distribution and number of the elements and nodes.
2. Solve the values of the U, V and θ at the steady state and regard them as the initial values.
3. Determine the time step $\Delta\tau$ and the mesh velocities $\hat{V}$ of the computational meshes.
4. Update the coordinates of the nodes and examine the determinant of the Jacobian transformation matrix to ensure the one-to-one mapping to be satisfied during the Gaussian quadrature numerical integration.
5. Solve Eq. (10), until the following criteria for convergence are satisfied:

$$\left|\frac{\phi^{m+1} - \phi^{m}}{\phi^{m+1}}\right|_{\tau+\Delta\tau} < 10^{-3}, \text{ where } \phi = U, V. \tag{14}$$

6. Substitute the U and V into Eq. (12) to obtain θ.
7. Continue the next time step calculation until the assigned amplitude of the fins is reached.

4. Results and discussion

The dimensionless geometric parameters are listed in Table 1. The working fluid is air with $Pr = 0.71$ and Reynolds number is varied from 500 to 1500. Several different swinging speeds of the fins, S_b, are evaluated and the maximum amplitude of the fins is assigned to be 0.05. Since the thickness of the fins D $(= 0.01)$ is very thin, the blockage effect and the heat transfer from the right and left surfaces of the fins can be neglected. The local Nusselt number $Nu_X(X, \tau)$ on the top or bottom surface of the fin is defined by the following equation:

Table 1
The dimensionless geometric parameters

H	H_1	H_2	D	W	W_1	W_2	W_3
7.0	3.085	0.4	0.01	15.0	4.0	1.0	10.0

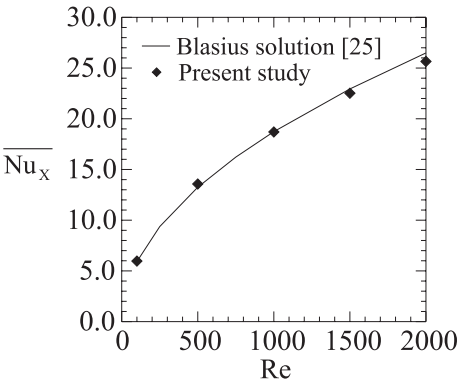

Fig. 2. Comparison of the results of the average Nusselt numbers on the top and bottom surfaces of the middle fin at steady state for different Reynolds numbers of the present study with the Blasius solution.

$$Nu_X(X,\tau) = -\frac{\partial\theta}{\partial Y}. \tag{15}$$

The average Nusselt number $\overline{Nu_X}(\tau)$ on the top or bottom surface of the fin is defined by

$$\overline{Nu_X}(\tau) = \frac{1}{W_2}\int_0^{W_2} Nu_X \, \mathrm{d}X, \tag{16}$$

where W_2 is the length of the fin. In addition, the overall average Nusselt number $Nu(\tau)$ of the fin is defined as

$$Nu(\tau) = \frac{1}{2W_2}\left(\int_0^{W_2} Nu_X|_{\text{top}} \, \mathrm{d}X + \int_0^{W_2} Nu_X|_{\text{bottom}} \, \mathrm{d}X\right). \tag{17}$$

For obtaining an optimal computational meshes, a series of numerical tests for various meshes at the steady state are executed. The nonuniform distribution of 3872 elements corresponding to 15 942 nodes is chosen. Since the pitch of the fins ($H_2 = 0.4$) is larger than the thickness of the fins ($D = 0.01$), the flow and thermal fields at the steady state are similar to the fluid flowing over a flat plate. The Blasius solution [25] for the average Nusselt number with laminar flow over a flat plate of length ι is

$$\overline{Nu_X} = 0.664 Re_\iota^{1/2} Pr^{1/3}. \tag{18}$$

In Fig. 2, the average Nusselt numbers on the top and bottom surfaces of the middle fin at the steady state

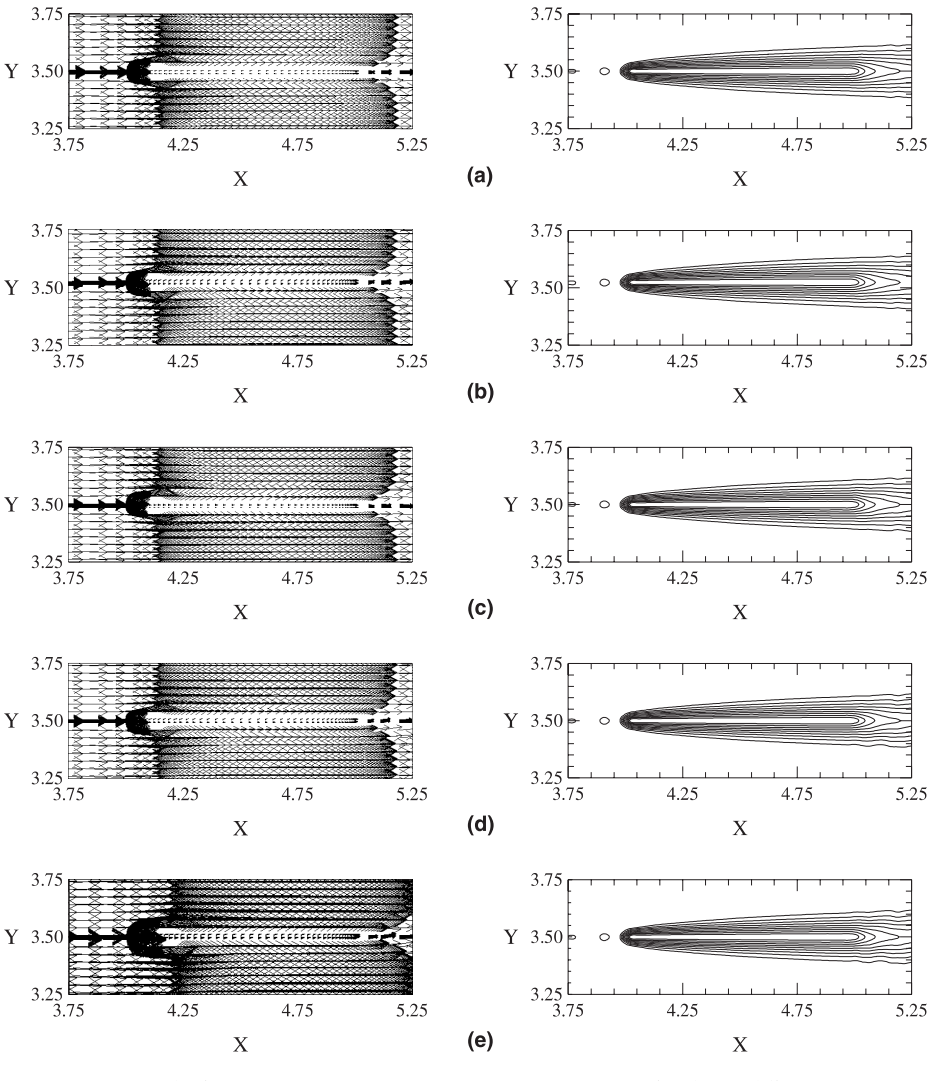

Fig. 3. The transient developments of the velocity vectors and isothermal lines around the middle fin for the swinging speed of the fins $S_b = 0.025$ and $Re = 1000$ case: (a) $\tau = 0.0$, (b) $\tau = 1.0$, (c) $\tau = 4.0$, (d) $\tau = 8.0$, and (e) $\tau = 24.0$.

for different Reynolds numbers are compared with those of the Blasius solutions. Both the results are consistent well. As for the time step $\Delta\tau$, the time step $\Delta\tau = 1.0 \times 10^{-2}$ is chosen for the swinging speed of the fins $S_b = 0.025$ case, and $\Delta\tau = 5.0 \times 10^{-3}$, 2.5×10^{-3} and 2.0×10^{-3} are chosen for the swinging speed of the fins $S_b = 0.5$, 1.0 and 2.0 cases, respectively. Besides, the residual of the continuity equation

$$\text{Residual} = \frac{\partial U}{\partial X} + \frac{\partial V}{\partial Y} \tag{19}$$

is checked for each element on each time to ensure the mass conservation law to be satisfied. In the computing processes, the residual of the continuity equation for each element is smaller than 1.0×10^{-6}.

For illustrating the variations of the flow and thermal fields more detailed, the middle fin is focused on and the velocity vectors and isothermal lines around the middle fin are presented only. However, it should be noted the computational domain included three swinging fins, and a much larger region was calculated than what is displayed in the subsequent figures. In addition, the velocity vectors shown in the following figures are scaled relatively to the maximum velocity in the flow field.

Fig. 3 present the transient developments of the velocity vectors and isothermal lines around the middle fin under the swinging speed of the fins $S_b = 0.025$ and $Re = 1000$ case. At the time $\tau = 0.0$, the fin is stationary and the fluid is flowing steadily, as shown in Fig. 3(a). As the time $\tau > 0$, the fins start in motion of swinging back and forth. As shown in Fig. 3(b), the fin is on the way to move upward. The fluid close to the top surface of the fin is pushed by the fin and flows upward. As a result, the heat transfer is enhanced. Conversely, the fluid near the bottom surface of the fin simultaneously replenishes the vacant space induced by the movement of the fin. Most of the fluid near the bottom surface of the fin are difficult to catch up to the bottom surface of the fin simultaneously, this flow is disadvantageous to the heat transfer. Afterwards, the fin moves upward continuously until the amplitude of the fin is equal to 0.05. The variations of the flow fields are similar to those of the flow fields mentioned above.

The motion of the fin turns downward immediately as the fin reaches the maximum upper amplitude. As shown in Fig. 3(c), the fin is on the way to move downward and the position of the middle fin is at the center of the channel. The fin pushes the fluid near the bottom surface of the fin, which is profitable for the heat transfer. In the meantime, the fluid close to the top surface of the fin continuously replenishes the vacant space near the top surface of the fin as the fin moves downward.

In Fig. 3(d), the fin is on the way to move upward and the position of the middle fin returns to the center of the channel. The variations of the flow fields are similar to those as shown in Fig. 3(b).

As the time increases, the fin swings back and forth as mentioned above. Since the fins swing with a small speed, the variations of the flow fields are slight.

As for the thermal fields, the variations of the thermal fields usually correspond to the variations of the flow fields. Since the swinging speed of the fin is very slow, the flow fields are similar to the fluid flowing over a flat plate. Thus, the variations of the thermal fields are very slight and the distributions of the isothermal lines are similar to those of the fluid flowing through a stationary plate.

Fig. 4(a) shows the variations of the average Nusselt number $\overline{Nu_X}$ on the top and bottom surfaces of the middle fin with time at the same conditions as shown in Fig. 3. Based upon these reasons mentioned earlier, as the fin moves upward, the average Nusselt number on the top surface of the fin increases slightly, but the

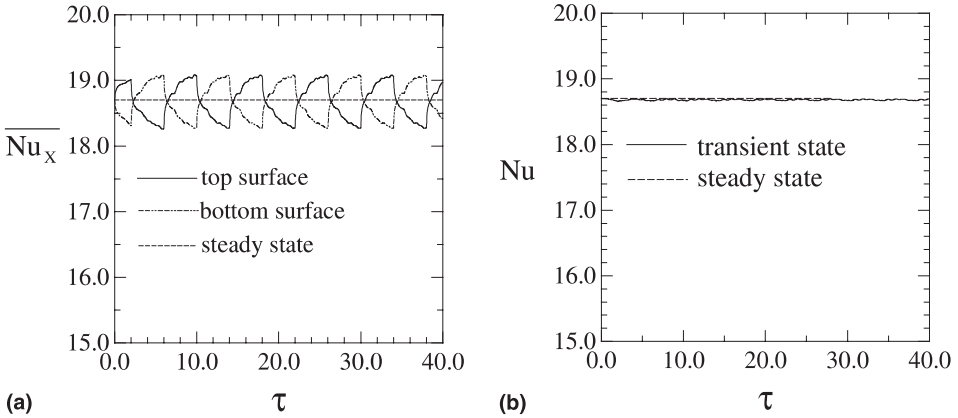

Fig. 4. The variations of the Nusselt number on the middle fin with time for the swinging speed of the fins $S_b = 0.025$ and $Re = 1000$ case: (a) the average Nusselt number $\overline{Nu_X}$, and (b) the overall Nusselt number Nu.

average Nusselt number on the bottom surface decreases. As the fin moves downward, the results of the variations of the average Nusselt number on the fin are opposite to those of the fin moving upward. The variations of the overall average Nusselt number Nu on the middle fin with time are very slight compared with the steady state, as shown in Fig. 4(b).

Fig. 5 shows the transient developments of the velocity vectors and isothermal lines around the middle fin under the swinging speed of the fins $S_b = 0.5$ and $Re = 1000$ case. Since the swinging speed of the fin is greater than that of the case above, the variations of the flow and thermal fields near the fin are more drastic in this case. As shown in Fig. 5(b) and (c), the fin is on the way to move upward. The fluid near the top surface on the fin is pushed by the fin and flows upward. In the meantime, the fluid close to the left and bottom surfaces of the fin fills the vacant space near the bottom surface of the fin induced by the movement of the fin. As a result, a small recirculation zone, which is disadvantageous to the heat transfer, and a reattachement flow, which is advantageous to the heat transfer, are observed around the left corner of the bottom surface of the fin. The distributions of the isothermal lines near the top

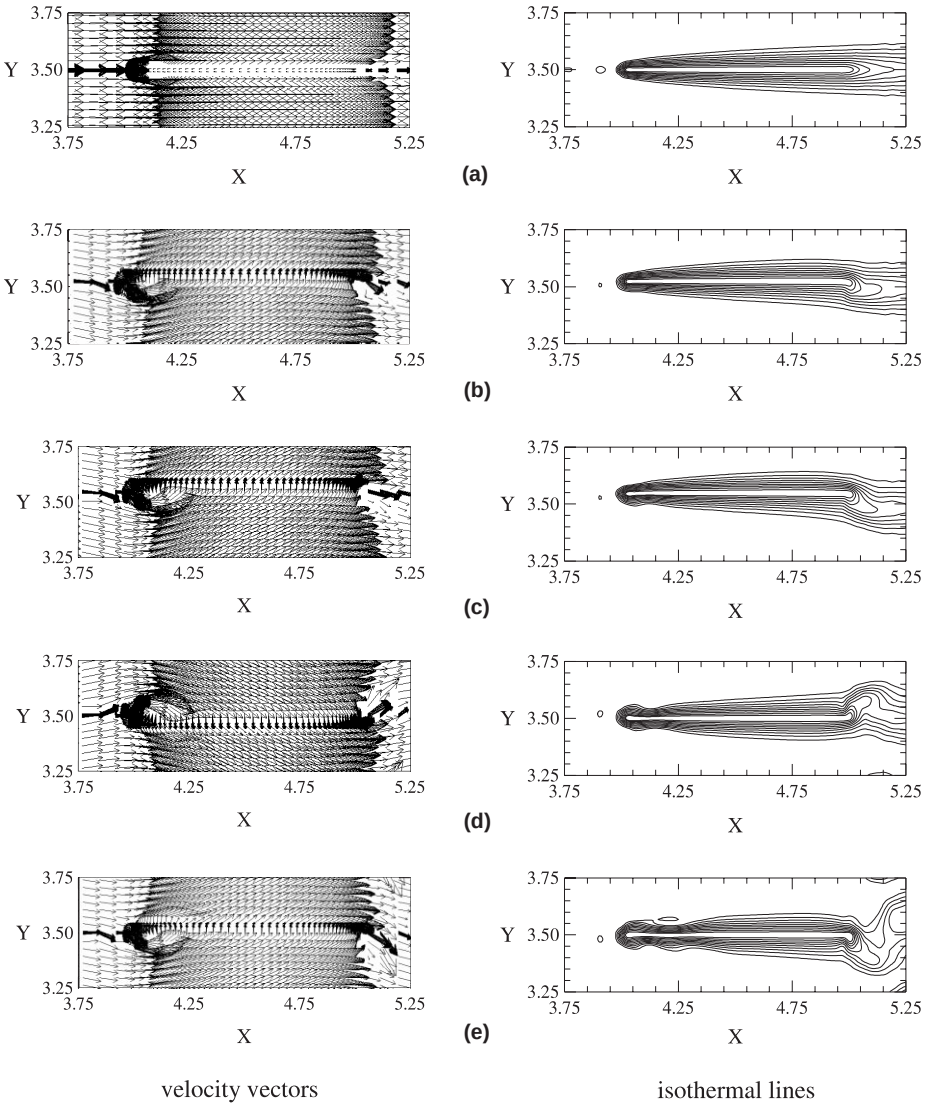

Fig. 5. The transient developments of the velocity vectors and isothermal lines around the middle fin for the swinging speed of the fins $S_b = 0.5$ and $Re = 1000$ case: (a) $\tau = 0.0$, (b) $\tau = 0.05$, (c) $\tau = 0.1$, (d) $\tau = 0.2$, (e) $\tau = 0.4$, (f) $\tau = 0.6$, (g) $\tau = 0.8$, (h) $\tau = 1.0$, (i) $\tau = 1.2$, and (j) $\tau = 5.6$.

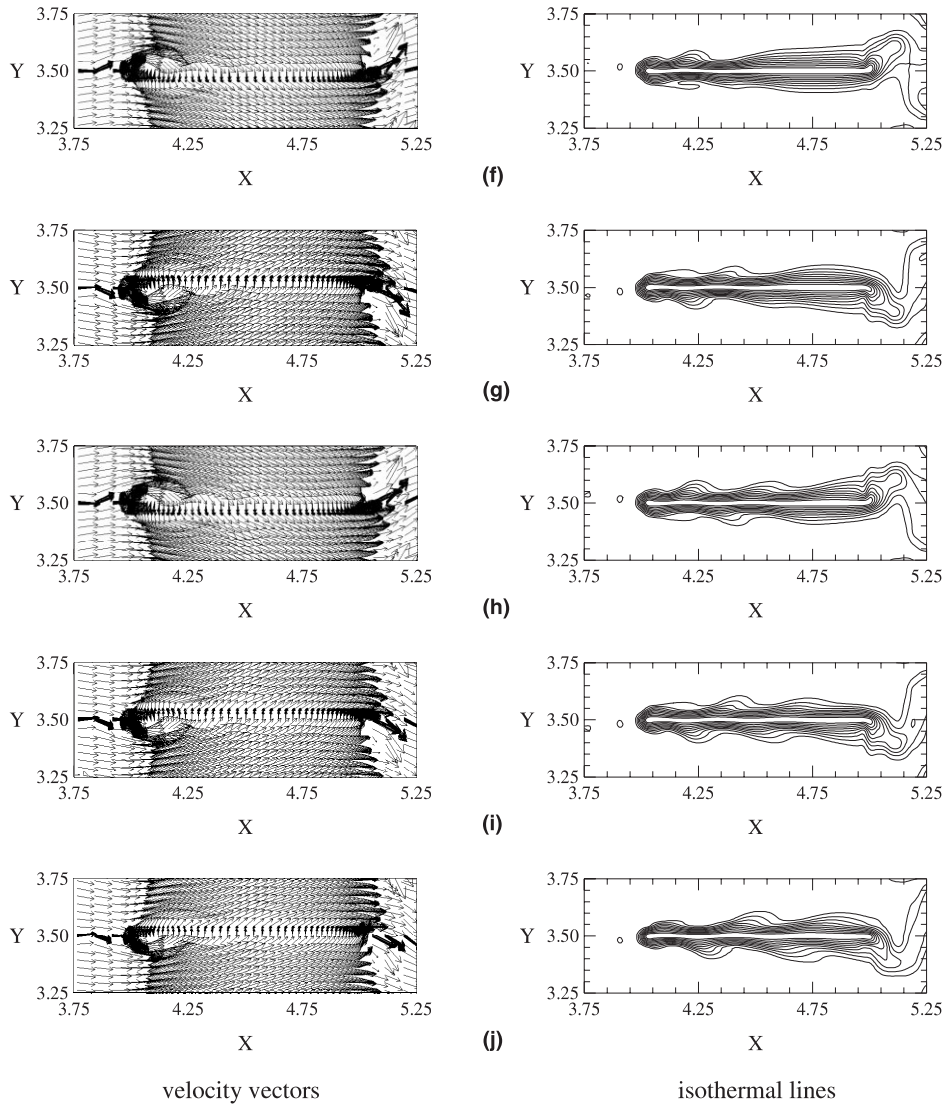

Fig. 5 (*continued*)

surface of the fin are denser than those of the bottom surface of the fin. Besides, the distributions of the isothermal lines become denser near the reattachement flow.

In Fig. 5(d), the fin is on the way to move downward and the position of the middle fin is at the center of the channel. Since the fin moves downward, the fin pushes the fluid near the bottom surface of the fin. Conversely, the fluid near the left and top surfaces of the fin continuously replenishes the vacant space near the top surface of the fin induced by the movement of the fin. As a result, a recirculation zone and a reattachement flow are formed around the left corner of the top surface of the fin. Similarly, the distributions of isothermal lines become denser near the reattachement flow and sparser near the recirculation zone around the left corner of the top surface of the fin.

As shown in Fig. 5(e)–(j), since the fin is in motion of swinging back and forth with a high swinging speed, the recirculation zones and reattachement flows are formed around the fin continuously and migrate to the downstream gradually, which may cause the boundary layers of the flow and thermal fields to be contracted and disturbed during the transient developments. Consequently, the heat transfer is enhanced remarkably.

The variations of the overall average Nusselt number Nu on the surfaces of the middle fin with time at the same conditions as shown in Fig. 5 are indicated in Fig. 6. According to the variations of the flow and thermal fields mentioned above, the overall average Nusselt

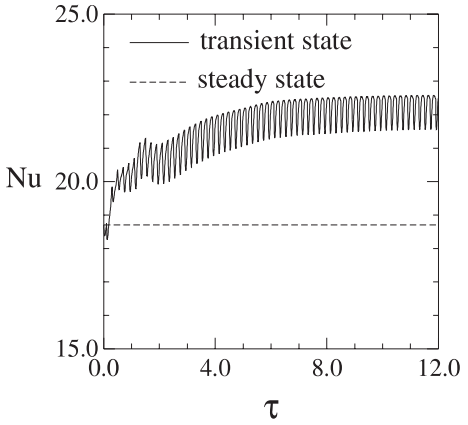

Fig. 6. The variations of the overall average Nusselt number Nu on the middle fin with time for the swinging speed of the fins $S_b = 0.5$ and $Re = 1000$ case.

number during the transient developments is enhanced remarkably. Furthermore, as the time increases, the flow and thermal fields may approach to a periodic state, and the mean increment of the overall average Nusselt number on the middle fin is about 15% in the computing range.

In addition, Fig. 7 shows the variations of the overall average Nusselt number Nu on the middle fin with time for various cases. Fig. 7(a) and (b) indicate the swinging speed of the fins $S_b = 1.0$ and 2.0 under $Re = 1000$ cases, respectively. The variations of the overall average Nusselt number with time are hardly found out to be periodic, this is suggested as that the swinging speed of the fin is too fast and the flow and thermal fields are unable to develop regular patterns in time. In the computing range, the mean increment of the overall average Nusselt number on the middle fin are about 50% and 120% in these two cases, respectively, which are larger than those of the cases above. As expected, the

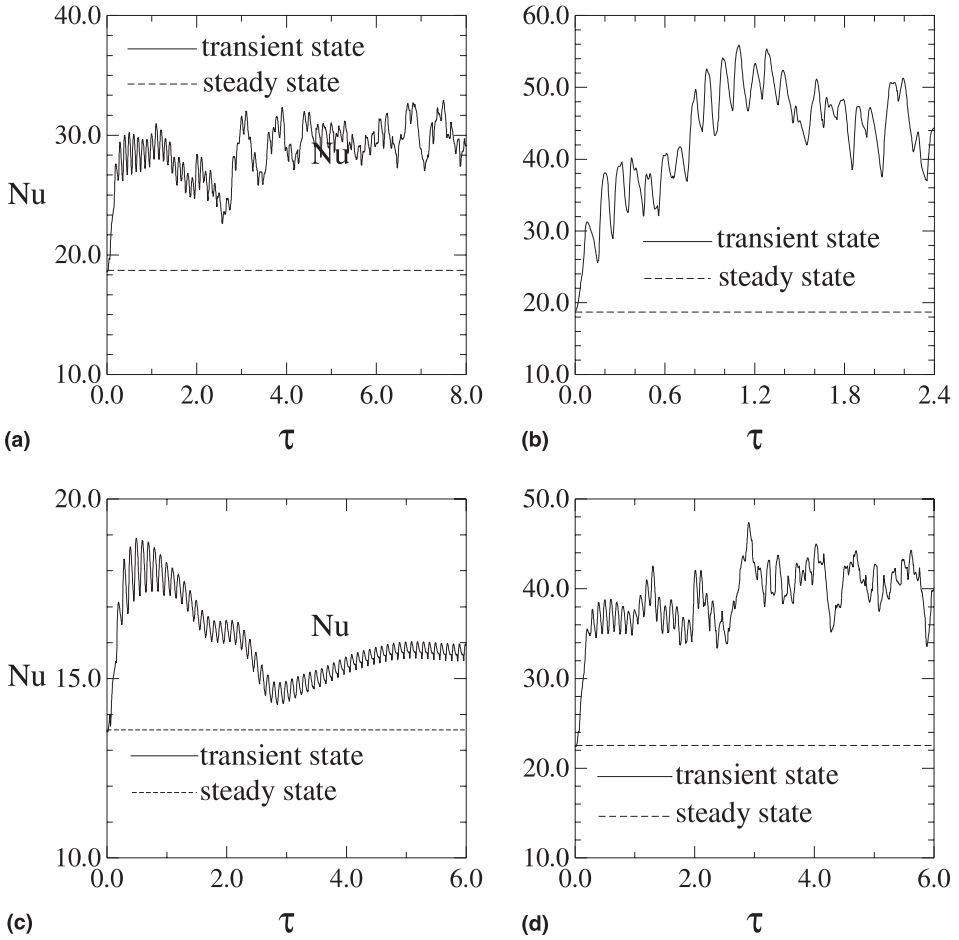

Fig. 7. The variations of the overall average Nusselt number Nu on the middle fin with time for various cases: (a) $Re = 1000, S_b = 1.0$, (b) $Re = 1000, S_b = 2.0$, (c) $Re = 500, S_b = 1.0$, and (d) $Re = 1500, S_b = 1.0$.

enhancement of the heat transfer increases significantly with increased the swinging speed of the fins.

Fig. 7(c) and (d) present the swinging speed of the fins $S_b = 1.0$ under $Re = 500$ and $Re = 1500$ cases, respectively. In the computing range, the mean increment of the overall average Nusselt number on the middle fin for these two cases are about 18% and 80%, respectively. As expected, the heat transfer increases with increased Reynolds number.

5. Conclusions

A numerical simulation for the heat transfer of extremely thin fins of a finned heat sink which swing back and forth induced by a flowing fluid or an oscillation exciter is presented. Some conclusions are summarized as follows:

1. As the fins swing with a small speed, the variations of the flow and thermal fields are slight and similar to the fluid flowing over a flat plate.
2. As the fins swing with a large speed, the recirculation zones and reattachement flows are formed around the fins continuously and migrate to the downstream gradually. This may cause the velocity and thermal boundary layers to be contracted and disturbed, which results in the enhancement of heat transfer remarkably.
3. As the fins swing with a relatively low speed, the variations of the flow and thermal fields may approach to regular patterns with time, which result in the variations of the overall average Nusselt number being a periodic state. However, the variations of the flow and thermal fields are unable to develop regular patterns with time as the fins swing with a large speed.

Acknowledgements

The support of this work by the National Science Council of Taiwan, R.O.C., under contract NSC89-2212-E-009-010 is gratefully acknowledged.

Appendix A

The photographs of the swinging of the fin induced by the flowing fluid are showed in Fig. 8. A finned heated sink with single extremely thin fin is set on the test section of a small wind tunnel. The extremely thin fin is made of Co-based amorphous ribbon and 25 μm in thickness. As shown in Fig. 8(a), both the fluid and fin are stationary. As shown in Fig. 8(b) and (c), the fluid flows through the tunnel. The extremely thin fin is then swinging induced by the flowing fluid. As a result, the images of the fin in the photographs are foggy.

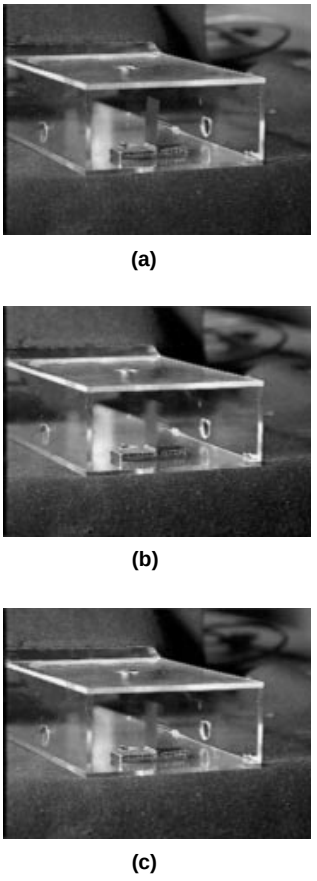

Fig. 8. The photograph of the swinging of the fin: (a) stationary, (b) and (c) in swinging situation.

References

[1] A.E. Bergles, Recently development in convective heat-transfer augmentation, Appl. Mech. Rev. 26 (1988) 675–682.
[2] R.L. Webb, Principles of Enhanced Heat Transfer, Wiley, New York, 1993 (Chapter 1).
[3] L.T. Yeh, Review of heat transfer technologies in electronic equipment, J. Electron. Packaging 117 (1995) 333–339.
[4] S. Sathe, B. Sammakia, A review of recent developments in some practical aspects of air-cooled electronic packages, J. Heat Transfer 120 (1998) 830–839.
[5] H.W. Markstein, New development in cooling techniques, Electron. Packaging Production 16 (1975) 36–44.
[6] S. Sathe, K.M. Karki, C. Tai, C. Lamb, S.V. Patanker, Numerical prediction of flow and heat transfer in an impingement heat sink, J. Electron. Packaging 119 (1997) 58–63.
[7] Y. Kondo, M. Behnia, W. Nakayama, H. Matsushima, Optimization of finned jet sinks for impingement cooling of electronic packages, J. Electron. Packaging 120 (1998) 259–266.
[8] K. Vafai, Z. Lu, Analysis of two-layered micro-channel heat sink concept in electronic cooling, Int. J. Heat Mass Transfer 42 (1999) 2287–2297.

[9] U.C. Saxena, A.D.K. Laird, Heat transfer from a cylinder oscillating in a cross-flow, J. Heat Transfer 100 (1978) 684–689.
[10] U.H. Kurzweg, Heat transport along an oscillating flat plate, J. Heat Transfer 110 (1988) 789–790.
[11] K. Shailendhra, S.P. Anjalidevi, Heat transport along oscillating flat plate in the presence of a transverse magnetic field, Int. J. Heat Mass Transfer 40 (1997) 498–501.
[12] C.H. Cheng, J.L. Hong, W. Aung, Numerical prediction of lock-on effect on convective heat transfer from a transversely oscillating circular cylinder, Int. J. Heat Mass Transfer 40 (1997) 1825–1834.
[13] Y. Haneda, Y. Tsuchiya, K. Nakabe, K. Suzuki, Enhancement of impinging jet heat transfer by making use of mechano-fluid interactive flow oscillation, Int. J. Heat Fluid Flow 19 (1998) 115–124.
[14] C.W. Hirt, A.A. Amsden, H.K. Cooks, An arbitrary Lagrangian–Eulerian computing method for all flow speeds, J. Comput. Phys. 14 (1974) 227–253.
[15] T.J.R. Hughes, W.K. Liu, T.K. Zimmermann, Lagrangian–Eulerian finite element formulation for incompressible viscous flows, Comput. Meth. Appl. Mech. Eng. 29 (1981) 329–349.
[16] J. Donea, S. Giuliani, J.P. Halleux, An arbitrary Lagrangian–Eulerian finite element method for transient dynamic fluid-structure interactions, Comp. Meth. Appl. Mech. Eng. 33 (1982) 689–723.
[17] B. Ramaswamy, M. Kawahara, Arbitrary Lagrangian–Eulerian finite element method for unsteady, convective, incompressible viscous free surface fluid flow, Int. J. Numer. Meth. Fluids 7 (1987) 1053–1075.
[18] W.S. Fu, S.J. Yang, Numerical simulation of heat transfer induced by a body moving in the same direction as flowing fluids, Heat Mass Transfer 36 (2000) 257–264.
[19] W.S. Fu, S.J. Yang, Heat transfer induced by a body moving in opposition to a flowing fluid, Int. J. Heat Mass Transfer 44 (2001) 89–98.
[20] J.N. Reddy, D.K. Gartling, The Finite Element Method in Heat Transfer and Fluid Dynamics, CRC Press, Boca Raton, 1994 (Chapter 4).
[21] W.S. Fu, T.M. Kau, W.J. Shieh, Transient laminar natural convection in an enclosure from steady flow state to stationary state, Numer. Heat Transfer A 18 (1990) 189–211.
[22] B.M. Irons, A frontal solution program for finite element analysis, Int. J. Numer. Meth. Eng. 2 (1970) 5–32.
[23] P. Hood, Frontal solution program for unsymmetric matrices, Int. J. Numer. Meth. Eng. 10 (1976) 379–399.
[24] H. Schlichting, Boundary Layer Theory, McGraw-Hill, New York, 1979 (Chapter 7).
[25] F.P. Incropera, D.P. Dewitt, Fundamentals of Heat and Mass Transfer, Wiley, New York, 1990 (Chapter 7).